J Fluoresc (2011) 21:1805–1811
DOI 10.1007/s10895-011-0875-6

ORIGINAL PAPER

Prism-Based Spectral Imaging of Single-Molecule Fluorescence from Gold-Nanoparticle/Fluorophore Complex

Tsuyoshi Sonehara · Tomoyuki Sakai · Takanobu Haga · Takeshi Fujita · Satoshi Takahashi

Received: 28 September 2010 / Accepted: 23 February 2011 / Published online: 8 March 2011

Abstract A wavelength-calibration method for prism-based spectral imaging of single-molecule (SM) fluorescence was developed. With this method, a wavelength reference is provided by photoluminescence from 50-nm-diameter gold nanoparticles (AuNPs) binding with fluorophores. The AuNPs each bound with a SM fluorophore, either Alexa488 or Cy3, to form AuNP/fluorophore complexes in tris-HCl buffer. Each complex was immobilized on a silica slide and then excited by total-internal-reflection illumination to make it emit SM fluorescence and AuNP photoluminescence. The portion of the AuNP photoluminescence transmitted by a band-pass filter gives the wavelength reference. A spectral-imaging system composed of a prism-based spectroscope (with a reciprocal dispersion of about 4 nm/μm) and a charge-coupled device with 6.45-μm-square pixels was used to obtain an SM-fluorescence spectrum and a wavelength-reference spectrum. Through smoothed differentiation of these two spectra, the peak location of the former in relation to the latter was determined with subpixel precision. After that, the SM fluorophore was classified as either Alexa488 or Cy3 according to the peak location. The error rate of the classification was estimated to be only 0.3%.

Keywords Wavelength calibration · Prism · Single molecule · Gold nanoparticle · Photoluminescence

T. Sonehara (✉) · T. Sakai · T. Haga · T. Fujita
Hitachi, Ltd., Central Research Laboratory,
1-280 Higashi-koigakubo,
Kokubunji, Tokyo 185-8601, Japan
e-mail: tsuyoshi.sonehara.wf@hitachi.com

S. Takahashi
Research and Development Division,
Hitachi High-Technologies Corporation,
882 Ichige,
Hitachinaka, Ibaraki 312-8504, Japan

Introduction

Spectral imaging of single-molecule (SM) fluorescence is a fundamental technique for a variety of biological experiments at the SM level. To detect weak SM fluorescence, these experiments require low-loss spectroscopy. There are two main types of theoretically lossless spectroscopy: the dichroic-mirror type and prism type. These two types of spectroscopy, which can be conducted without mechanical movement of optics, provide high sensitivity and high temporal resolution. Taking advantage of these features, various systems has been developed [1–5]. Many of them are two-color systems of the dichroic-mirror type [1–3]. The system configuration of this type, however, rapidly becomes complex as the number of colors to be spectrally resolved increases. This is disadvantageous in regard to SM experiments resolving three colors or more. In contrast, the prism type has the advantage that its system configuration depends little on the number of colors.

In prism-based spectral imaging, the fluorescence spectrum of a SM fluorophore, which is generally immobilized on a slide, is given as a pixel-value array along a line in an image; in other words, the line provides the wavelength axis for the spectrum. Unfortunately, this axis cannot be calibrated by using the spectrum itself unless its wavelength range is known. When the fluorophore species is unknown, the axis calibration requires a wavelength marker, namely, the point source with a known emission wavelength at the same position as the fluorophore. Normal methods of immobilizing fluorophores, however, do not provide the wavelength marker. Moreover, high spectral resolution cannot readily be obtained in prism-based spectroscopy of SM fluorescence because it decreases fluorescence detected at a pixel and thus makes images noisy. For the reasons described above, prism-based spectral imaging has not been

widely used for SM experiments that require fluorophore classification by spectrum.

Several groups have reported on fluorescence enhanced by binding fluorophores with metal nanostructures such as gold nanoparticles (AuNPs) [6–8], silver nanoparticles [9–12], and silver islands [13]. Since these metals themselves emit inherent photoluminescence [14–17], their nanostructures can be point sources with known emission wavelength at the same positions as the fluorophores. They can therefore be not only fluorescence enhancers but also wavelength markers in prism-based spectral imaging of SM fluorescence.

In this work, we demonstrate the ability of 50-nm AuNPs as wavelength markers. More precisely, a portion of the AuNP photoluminescence transmitted by a band-pass filter (BPF) is used as the wavelength reference. The peak location of the SM fluorescence spectrum in relation to the spectrum of the BPF-transmitted AuNP photoluminescence (reference spectrum) is determined. The goal of this work is to assess the accuracy of fluorophore classification according to the peak location.

Each of the AuNPs binds with a 50-mer DNA molecule labeled with either Alexa488 or Cy3 to form an AuNP/fluorophore complex. The complexes are immobilized on a silica slide and then excited by total-internal-reflection (TIR) illumination to emit SM fluorescence and AuNP photoluminescence. The SM fluorescence spectrum and reference spectrum are obtained by using a prism-based spectral-imaging system in which a pixel corresponds to a wavelength of about 25 nm. Although this spectral resolution is rather poor, smoothed differentiation of the spectra makes it possible to determine the peak location with subpixel precision. The SM fluorophore binding with the AuNP is classified as either Alexa488 or Cy3 according to peak location. Then, the error rate of the classification is statistically estimated.

Experimental

General

The 50-nm AuNP stock solution of 0.0068 wt.% (89 pM) was purchased from Tanaka Kikinzoku Kogyo K. K. (Japan). The sequence of the 50-mer fluorescently labeled ssDNA is 5′-AGTCGAGCGGTAGCACAGAGAGCTTGCTCTCGGGTGACGAGCGGCGGACG-3′.

The ssDNA with Alexa488 at the 5′ end and thiols at the 3′ end was synthesized by Japan Bio Service. The ssDNA with Cy3 at the 3′ end and thiols at the 5′ end and its unlabeled complementary were synthesized by Sigma Aldrich Japan. Bis(p-sulfonatophenyl) phenylphosphine dihydrate dipotassium salt (BSPP), cetyltrimethylammonium bromide (CTAB), and NaCl were purchased from Wako Chemical (Japan). Stock solutions of buffers were purchased from Promega Corporation (USA). All aqueous solutions were prepared with purified water (with resistance greater than 17.6 MΩ) made by an ultra-pure water-manufacturing device (LV-608, Toray, Japan) and percolated through syringe filters with 0.1-μm-diameter pores (Whatmann Inc, USA) prior to use. All processes were performed at room temperature.

Preparation of AuNP/Fluorophore Complex

Solutions were mixed in 1.5-mL reaction tubes, shaken at 750 rpm with a rotary shaker (SI-300C, As-One), and spun down at 13,200 rpm with a centrifuge and rotor (5415D and F45-24-11, Eppendolf, Germany). For each labeled DNA, a AuNP/fluorophore complex solution was prepared in the following four steps. First, AuNP solution containing 1-mg/mL BSPP was prepared by mixing 10 μL of 100-mg/dL BSPP solution and 990 μL of AuNP stock solution and shaken for 4 h. (The BSPP prevents the AuNPs from aggregating.) Second, after concentrating AuNP to 1 nM by spinning down the AuNP solution for 3 min and removing 890 mL of the supernatant, a solution containing 1-nM AuNP, 10-mM NaCl, and 11-nM labeled DNA was prepared by mixing the residual liquid, 0.9 μL of 1-M NaCl solution, and 1 μL of 1-μM DNA solution, and shaken for 20 h. As a result of this procedure, roughly a tenth of the AuNPs bind with a DNA through the mercapto group (−SH) of thiols. Third, after diluting 20 μL of the mix with 1-mg/dL BSPP solution to 50-fold, the dilution was concentrated by one-tenth by spinning down for 2 min and removing the supernatant. Fourth, three cycles of ten-fold dilution with 1-mg/dL BSPP solution, spinning down for 2 min, and ten-fold concentration are performed to remove unbound DNA.

Immobilization of AuNP/Fluorophore Complexes on Silica Slide

A thin channel was made by sandwiching two 25-μm-thick spacers (Lumirror 25-S10, Toray, Japan) between a silica slide (50×26×0.9 mm^3, Hikari Kobo, Japan) and a coverslip (18×18 mm^2, Matsunami Glass, Japan). The channel was filled with the solutions by depositing a droplet of them at the channel entrance and sucking it from the exit with filter papers (No. 3 Circle 150 mm, Toyo Roshi Kaisha, Japan). AuNP/fluorophore complexes were immobilized on the slide in the following steps: the channel is filled with 10 μL of 0.8-mM CTAB solution for 3 min, flushed with 100 μL of Tris-HCl buffer, filled with 10 μL of a complex solution (prepared as explained in the preceding section) for 3 min, flushed with 100 μL of tris buffer, filled with 10 μL of 3.4×SSC (saline-sodium citrate)

buffer containing 200-nM unlabeled complementary DNA for 1 h, and flushed with 100 μL of Tris-HCl buffer. The coverslip side was then closed up with a top coat (Keshowakusei, Shiseido Company, Japan). A slide with AuNP/Alexa488 complexes (hereafter, "Alexa488 slide") and a slide with AuNP/Cy3 complexes ("Cy3 slide") were prepared separately. Figure 1 schematically shows a completed slide; the balloon is a close-up of an AuNP/fluorophore complex.

Spectral Imaging

Figure 2 is a block diagram of the prism-based spectral-imaging system. The beam from a continuous-wave Ar-ion laser oscillating at 488 and 514.5 nm simultaneously (2214-40MLA, Uniphase, USA) passes through a focusing lens and TIR prism, on which either the Alexa488 slide or the Cy3 slide is located. A shutter repeatedly turns the beam on and off. Entering the slide through a glycerol layer between the TIR prism and the slide, the beam is totally reflected at a reflection angle of 69° on the complex-immobilized surface of the slide and generates an evanescent field. The total power and $1/e^2$ diameter of the beam just before the TIR are 30 mW and 0.2 mm, respectively. Each complex is excited by the evanescent field and emits SM fluorescence, AuNP photoluminescence, and scattered light. These emissions are collected by a microscope objective lens with a numerical aperture (NA) of 0.9 and focal length of 4.5 mm (UPlanApo 40×/0.9, Olympus, Japan), and the scattered light is rejected by a long-pass filter, LPF (LP02-514RU-25, Semrock, USA). A BPF with center wavelength of 590 nm and bandwidth of 40 nm is taken out and put in from the imaging system depending on the type of images to be acquired. Passing through a dispersing prism of BK7 with a wedge angle of 3°52′ (45559-I, Edmund Optics, USA) and an imaging lens with a focal length of 85 mm

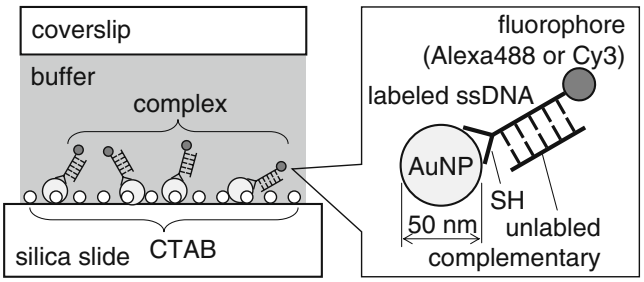

Fig. 1 Schematic illustration of a completed sample slide. Gold nanoparticle (AuNP) and fluorophore complexes in Tris-HCl buffer are immobilized on a silica slide through cetyltrimethylammonium bromide (CTAB) molecules. The *balloon* shows a close-up of a complex. A 50-mer ssDNA labeled with a single-molecule (SM) fluorophore at one end and thiols at the other end binds with a 50-nm AuNP through a mercapto group (−SH). The fluorophore is Alexa488 or Cy3. The labeled ssDNA forms a dsDNA with its unlabeled complementary

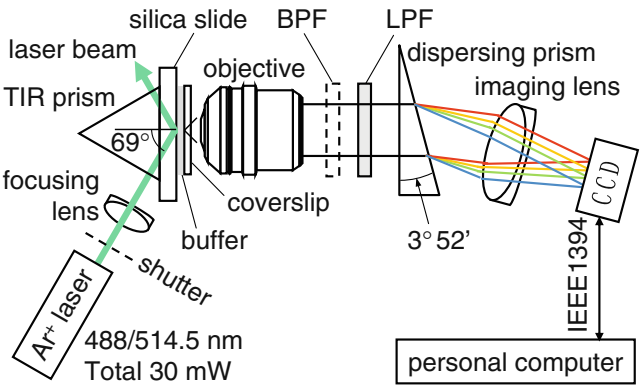

Fig. 2 Block diagram of the spectroscopy system. TIR, BPF, LPF, and CCD stand for total internal illumination, band-pass filter, long-pass filter, and charge-coupled device, respectively. Signal images are acquired without the BPF and reference images with it. The former images give SM fluorescence spectra and the latter reference spectra

(47640-I, Edmund Optics, USA), the SM fluorescence and AuNP photoluminescence form images on a charge-coupled device, CCD, with 1344×1024 6.45×6.45 μm^2 pixels (C4752-12-AG, Hamamatsu, Japan). The dispersing prism is set so that spectra are dispersed along the longer-side direction of the CCD imaging area. This direction is called the x-direction and its orthogonal, the y-direction. The CCD operating in continuous shoot mode generates 12-bit digital images at a frame interval of 0.24 s. The images are uploaded to the hard disc of a personal computer through an IEEE1394 interface.

For each slide, two sets of images were acquired: one set of the whole emissions (signal images), and another set of the BPF-transmitted photoluminescence (reference images). The signal images were acquired without the BPF for 60 s immediately after the shutter was opened. After that, the reference images were acquired for 6 s with the BPF put in.

Results and Discussion

Preliminary Definition and Calculations

Prior to reviewing some experimental results on the spectral-imaging system, some theoretical calculations are presented. First, the peak location, Δx, of the SM fluorescence spectrum for an AuNP/fluorophore complex is defined. As described above, an emission spectrum is dispersed along the x-direction of a spectral image; Δx is thus defined as

$$\Delta x \equiv x_F - x_R, \tag{1}$$

where x_F denotes the x-coordinate of the peak of the SM fluorescence spectrum, and x_R denotes that of the reference spectrum. Since the spectra are actually discrete pixel-value sequences, a decimal value of Δx cannot be directly obtained

from them. A way of obtaining the decimal peak location is presented in the next chapter.

It is assumed that the fluorophore is a monochromatic point source with a wavelengths of λ and that the AuNP with the BPF-transmitted photoluminescence is one with a wavelength of λ_c=590 nm. Accordingly, the relation between Δx and λ is given as shown in Fig. 3. The dispersing prism and imaging lens compose a spectroscope with a reciprocal dispersion of approximately 4 nm/μm around 590 nm. Moreover, the objective lens and imaging lens compose a lens system with a magnification of 19. The diffraction-limited image diameter of an AuNP is given by 19×1.22 λ_c/NA as 15 μm (i.e., 2.3 pixels).

Image Analysis

Figure 4 shows a signal image (a) and a reference image (b) of the Alexa488 slide. The two images display a common 80×60-pixel area of the whole images, which corresponds to a 27×20-μm^2 area of the slide. As shown in Fig. 4, many bright spots are observed in the Alexa488 slide. Similarly, many spots are observed in the Cy3 slide. The right side of a spot corresponds to longer wavelength. The spots in the reference image, which did not vanish after 60-s excitation, are photoluminescence images of individual AuNPs. The spots in the signal images (signal spots) are horizontally long because of spectral dispersion, while those in the reference images (reference spots) are approximately circular because the spectra were narrowed by the BPF. These reference spots were used to obtain wavelength references. On the basis of their spatial random distribution, pairs composed of a signal spot and a reference spot for identical AuNPs can be easily found, as shown in Fig. 4 as a1-b1, a2-b2, and a3-b3.

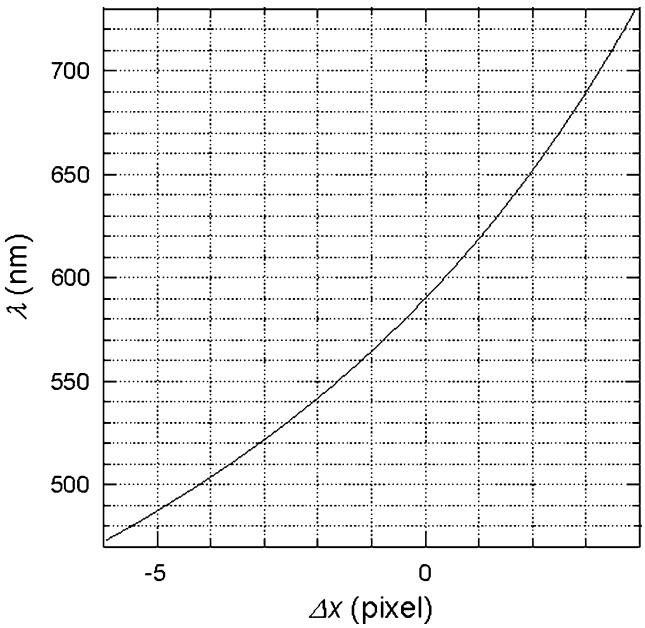

Fig. 3 Theoretically computed relation between the peak location of the SM fluorescence spectrum, Δx, and wavelength of the fluorophore, λ

As described above, roughly a tenth of the AuNPs are AuNP/fluorophore complexes. SM fluorescence images are superimposed on the spots of the complexes. In these spots, pixel-value vertical drops within the frame interval (0.24 s) due to photobleaching of fluorophores are observed. Figure 5 shows a typical vertical drop in pixel value in an AuNP/Alexa488 complex spot. On the basis of the vertical drop, the complex spots were extracted from all the spots.

The detailed analysis procedure for the images of a slide is composed of the following eight steps. Step (1): All images are convoluted with the 3×3 scalar matrix. Step (2): All the reference images are averaged to an image. The pixel value of the averaged image at the coordinate (x, y) is denoted by $R(x, y)$, and that of the i-th signal image by $S_i(x, y)$. Step (3): AuNP spots are extracted as continuous regions of the averaged reference image where $R(x, y)$ is larger than a threshold. The reference coordinate for a spot is determined as the rounded coordinate of its center of mass, which is denoted by (X, Y). Step (4): If a pixel-value vertical drop of the signal images is found in the region $\{(x, Y)|X-5\le x\le X+3\}$, the spot is judged to be a complex spot. Step (5): For a complex spot, the i-th signal spectrum is defined by the sequence $S_{ix}=S_i(X + x, Y)$, and the reference spectrum is defined by the sequence $R_x = R(X + x, Y)$ $(-7\le x\le 5)$. Step (6): The SM fluorescence spectrum is defined as the difference between the mean of five signal spectra obtained before the photobleaching and the mean of 20 signal spectra obtained after the photobleaching. Step (7): The integer peak location, Δi, is defined as i_F–i_R, where i_F denotes the peak index of the SM fluorescence spectrum, and i_R denotes that of the reference spectrum. Step (8): The decimal peak location, Δx, is defined as x_F–x_R, where x_F denotes the zero-crossover point of the smoothed differentiation of the SM fluorescence spectrum, and x_R denotes that of the reference spectrum. The smoothed differentiations are calculated using the Savitzky-Goray algorithm with five data points [18]. Figure 6 schematically shows steps 6–8.

Histograms and Statistics of Peak Location Figure 7(a) and (b) respectively show the histograms of Δi and those of Δx, both of which were obtained from a common set of AuNP/fluorophore-complex samples. The AuNP/Alexa488 complexes and tthe AuNP/Cy3 complexes are abbreviated to "Alexa488" and "Cy3," respectively. The gray bars represent 82 Alexa488 samples, and transparent bars represent 79 Cy3 samples. Naturally, Δi takes discrete integers only. In Fig. 7(a), eleven Alexa488 samples and 26 Cy3 samples stay together at exactly −1. On the one hand, Δx takes continuous values, though the abscissa step in

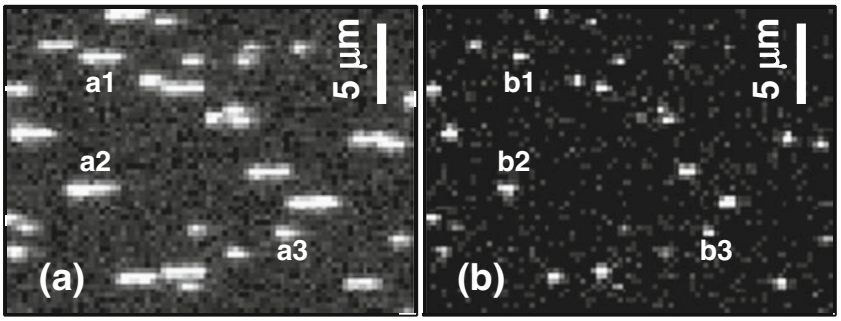

Fig. 4 Signal image (**a**) and reference image (**b**) for the Alexa488 slide. Each pair of spots, a*i* and b*i* (*i*=1–3), is due to an identical AuNP

Fig. 7(b) is set at 0.2 because of the finite number of samples. The two histograms of Δx are completely separated except for one Alexa488 sample. This result indicates the advantage of Δx over Δi in regard to threshold-based species classification, the details of which are described below.

Lets' consider we don't know which species a sample in Fig. 7 belongs to, Alexa488 or Cy3, though we actually know because the two slides were prepared separately. A threshold to classify the sample is then set according to Δi or Δx. If Δi (or Δx) is smaller than the threshold, the sample is classified as Alexa488; otherwise, it is classified as Cy3. Classification according to Δi is described first. If the threshold is set at −1, 100% of the Cy3 samples are correctly classified but 11/82 (i.e., 13%) of the Alexa488 samples are erroneously classified as Cy3. If the threshold is set at zero, 100% of the Alexa488 samples are correctly classified but 26/79 (i.e., 33%) of the Cy3 samples are erroneously classified as Alexa488. As long as Δi is used, higher accuracy cannot be obtained at any other threshold. Classification by Δx is described next. The valley of the two histograms in Fig. 7(b) locates at approximately −1, which must be an appropriate threshold. When the threshold is set at −1, 81/82 (i.e., 98.6%) of the Alexa488 samples and 79/79 (i.e., 100%) of the Cy3 samples are correctly classified. Only one of 82 Alexa488 samples (i.e., 1.2%) is erroneously classified as Cy3. The accuracy of species classification is thus greatly improved by using the decimal peak location. This improvement also demonstrates the effectiveness of the smoothed differentiation.

Table 1 lists the statistical parameters of Δx obtained from the samples in Fig. 7(b). According to Fig. 3, the means of Δx, −1.91 for Alexa488 and −0.25 for Cy3 correspond to 543 and 583 nm, respectively. These values are about 20 nm longer than the literature values of the peak wavelength, namely, 519 and 566 nm (http://www.invitrogen.com/site/us/en/home/support.html). The discrepancies in the values are

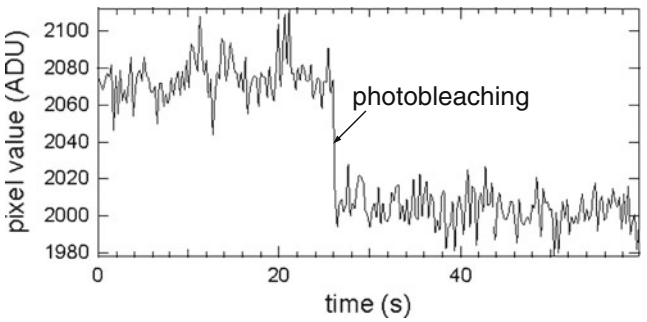

Fig. 5 Typical time course of the pixel value of an AuNP/Alexa488-complex spot. The vertical drop in pixel value is due to photobleaching of the Alexa488

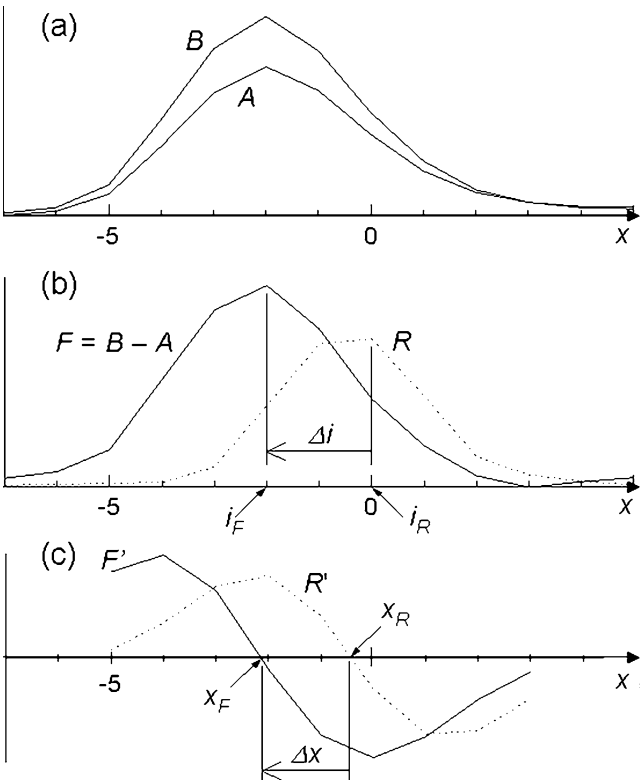

Fig. 6 Procedure for computing the peak location of the SM fluorescence spectrum: **a** The averages of the five signal spectra before photobleaching (*B*) and 20 signal spectra after photobleaching (*A*). **b** The SM fluorescence spectrum defined by *B*–*A* (*F*) and reference spectrum (*R*). The integer peak location, Δi, is defined by i_F–i_R, where i_F denotes the peak index of *F*, and i_R denotes that of *R*. **c** The smoothed differentiations of *F* (*F*′) and *R* (*R*′). The decimal peak location, Δx, is defined by x_F–x_R, where x_F denotes the zero-crossover point of *F*′ and x_R denotes that of *R*′

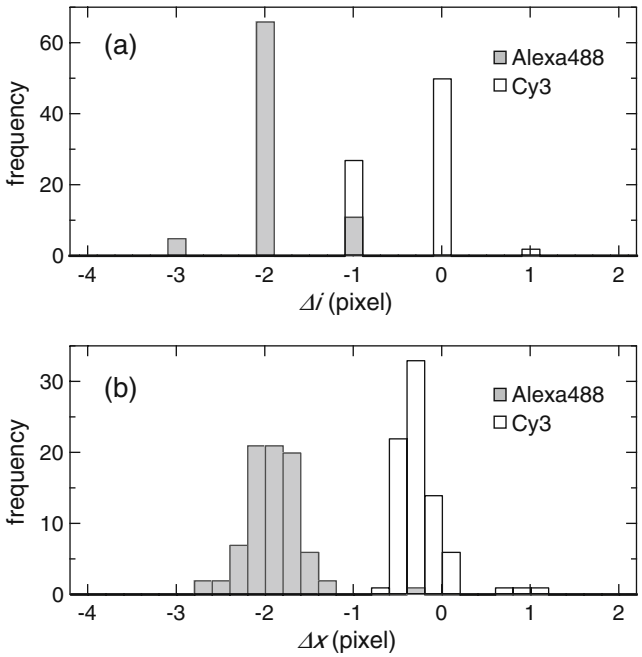

Fig. 7 Histograms of Δi (**a**) and those of Δx (**b**) obtained from a common set of AuNP/fluorophore-complex samples. The gray bars represent 82 Alexa488 samples, and the transparent bars, 79 Cy3 samples

probably due to smoothing. Note that spectra are smoothed not only by software but also by hardware. In the imaging hardware, a pixel corresponds to wavelength of about 25 nm, and the diffraction-limited spot size is larger than two pixels. Experimentally obtained raw spectra are therefore considerably smoothed. When the asymmetric fluorescence spectrum (with a larger "skirt" on the long-wavelength side) is smoothed, its apparent peak shifts to a longer wavelength. The reference spectrum, which is clipped from the original broad spectrum by the BPF, is narrower and more symmetric than the fluorescence spectrum. The peak shift for the former, therefore, must be larger than that for the latter. As a result, the peak locations shift to longer wavelengths. The effective fluorescence spectrum of Alexa488 is especially asymmetric because the original peak wavelength is close to the LPF cut-off, i.e., 520 nm. This result is consistent with the somewhat larger peak-wavelength discrepancy for Alexa488. On the other hand, the standard deviations of Δx of about 0.3 pixels show the decimal peak location was determined successfully with subpixel precision. They correspond to wavelength of about 7 nm. It is thus concluded that the system can determine the peak wavelength of the SM fluorescence not very accurately but fairly precisely.

Table 1 Statistical parameters of decimal peak location, Δx

Species (number of samples)	Alexa488 (82)	Cy3 (79)
Mean (pixel)	−1.91	−0.25
Standard deviation (pixel)	0.33	0.28

Estimation of Classification Error Rate

Each histogram in Fig. 7(a) gives a sample distribution of the probability distribution of a probability variable, Δx, for Alexa488 or Cy3. As explained in the following, the classification error rate determined by the probability distributions was statistically estimated according to an extension of a general theory [19].

Lets' consider the signal S obtained by analyzing a sample, which belongs to one of the two species, A and B. It is assumed that values of S for a species distribute according to a Gaussian function. As mentioned in the preceding section, the sample is classified according to the magnitude relation between S and a threshold, S_C. If $S < S_C$, the sample is classified as A, otherwise, as B. Figure 8 illustrates this classification procedure. The notations, C_X, S_X, and σ_X denote the probability distribution, mean, and standard deviation of S for species X, respectively (X = A, B). In the classification procedure, two errors can occur: classifying A as B or classifying B as A. The former error rate is given as the diagonally shaded area (α), and the latter as the stippled area (β). Naturally, S_C is set so that $\alpha=\beta$, unless one of the two errors is especially important. The value of S_C is given by

$$S_C = \frac{\sigma_A S_B + \sigma_B S_A}{\sigma_A + \sigma_B}, \tag{2}$$

and the error rate common to both the errors is given by

$$\alpha = \beta = \Phi(-2R_S), \tag{3}$$

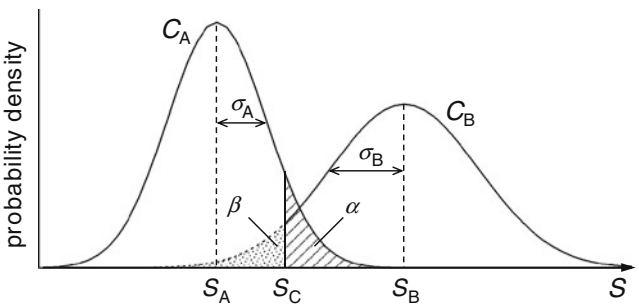

Fig. 8 Illustration of the classification of samples into A and B by S. The notations, C_X, S_X, and σ_X denote the probability distribution, mean, and standard deviation of S for species X, respectively (X = A, B). If $S<S_C$, a sample is classified as A; otherwise, it is classified as B. The diagonally shaded area (α) denotes the error rate of classifying an A sample as B; the stippled area (β) denotes that of classifying a B as A

where Φ is the cumulative distribution of the standard normal distribution, $\Phi(z) \equiv \frac{1}{\sqrt{2\pi}} \int_{-\infty}^{z} \exp(-x^2/2)dx$, and R_S is the resolution defined by

$$R_S \equiv \frac{S_B - S_A}{2(\sigma_A + \sigma_B)}, \quad (4)$$

which is equivalent to that for chromatograms.

The above-described theory can be applied to fluorophore classification by considering S, A, and B to be Δx, Alexa488, and Cy3, respectively. The mean values and standard deviations of the probability distributions are estimated by those of the sample distributions listed in Table 1. Substituting the values into Eqs. 2 to 4 gives S_C= 1.01, R_S=1.34, and α=β=0.3%. This value of S_c agrees well with that used in the preceding section, namely, −1, which was determined by visual observation of the histograms. Moreover, in consideration that general qualitative determination between positive and negative is often conducted with an error rate of 5%, it is concluded that the error rate of 0.3% is sufficiently small for various applications.

Concluding Remarks

A wavelength-calibration method was developed for prism-based spectral imaging of single-molecule (SM) fluorescence. The peak location of the SM fluorescence spectrum for a gold nanoparticle (AuNP)/fluorophore complex was determined by using a band-pass-filter (BPF)-transmitted AuNP photoluminescence spectrum. Accordingly, accurate fluorophore classification by peak location was demonstrated. Although this experimental demonstration was limited to the case of two species of fluorophores, Alex488 and Cy3, it can easily be expanded to three species or more. If the peaks of the fluorescence spectra of the other species are spaced as far as those of Alexa488 and Cy3, comparable classification accuracy will be obtained without having to change the imaging-system configuration. Despite the low spectral resolution of the imaging system, smoothed differentiation of fluorescence spectra made it possible to precisely determine the peak wavelength of the florescence spectra. It should be noted that this low resolution allows high-density fluorophore implantation on a slide as well as high-sensitivity detection of fluorophores. The authors believe this new wavelength-calibration method will become a basic technique for applications classifying densely-implemented multicolor SM fluorophores.

Acknowledgments We thank Dr. Miwako Nakahara and Dr. Osamu Kogi for their helpful advice on sample preparation.

References

1. Murakoshi H et al (2004) Single-molecule imaging analysis of Ras activation in living cells. Proc Natl Acad Sci USA 101:7317–7322
2. Friedman LJ et al (2006) Viewing dynamic assembly of molecular complexes by multi-wavelength single-molecule fluorescence. Biophys J 91:1023–1031
3. Kang SH et al (2007) Detection of single-molecule DNA hybridization by using dual-color total internal reflection fluorescence microscopy. Anal Bioanal Chem 387:2663–2671
4. Suzuki Y et al (2002) Imaging of the fluorescence spectrum of a single fluorescent molecule by prism-based spectroscopy. FEBS Lett 512:235–239
5. Lundquist PM et al (2008) Parallel confocal detection of single molecules in real time. Opt Lett 33:1026–1028
6. Anger P et al (2006) Enhancement of quenching of single-molecule fluorescence. Phys Rev Lett 96:113002
7. Kühn S et al (2006) Enhancement of single-molecule fluorescence using a gold nanoparticle as an optical nanoantenna. Phys Rev Lett 97:017402
8. Bek A et al (2008) Fluorescence enhancement in hot spots of AFM-designed gold nanoparticle sandwiches. Nano Lett 8:485–490
9. Fu Y et al (2008) Reduced blinking and long-lasting fluorescence of single fluorophores coupling to silver nanoparticles. Langmuir 24:3429–3433
10. Zhang J et al (2007) Metal-enhanced single-molecule fluorescence on silver particle monomer and dimmer: coupling effect between metal particles. Nano Lett 7:2101–2107
11. Fu Y et al (2007) Plasmonic enhancement of single-molecule fluorescence near a silver nanoparticle. J Fluoresc 17:811–816
12. Ray K et al (2008) Single-molecule spectroscopic study of enhanced intrinsic phycoerythrin fluorescence on silver nanostructured surfaces. Anal Chem 80:6942–6948
13. Fu Y, Lakowicz JR (2006) Enhanced fluorescence of Cy5-labeled DNA tethered to silver island films: fluorescence images and time-resolved studies using single-molecule spectroscopy, (2006). Anal Chem 78:6238–6245
14. Mooradian A (1969) Photoluminescence of metals. Phys Rev Lett 22:185–187
15. Zhao Y et al (2006) Spectroscopy property of Ag nanoparticles. Spectrochim Acta A Mol Biomol Spectrosc 65:1003–1006
16. Tamaru H et al (2002) Resonant light scattering from individual Ag nanoparticles. Appl Phys Lett 80:1826–1828
17. Bouhelier A et al (2005) Surface plasmon characteristics of tunable photoluminescence in single gold nanorods. Phys Rev Lett 95:267405
18. Savitzky A, Golay MJE (1964) Smoothing and differentiation of data by simplified least-squares procedures. Anal Chem 36:1627–1639
19. Currie LA (1968) Limits for qualitative detection and quantitative determination. Anal Chem 40:586–593